Chemical Science

ROYAL SOCIETY OF CHEMISTRY

PERSPECTIVE

View Article Online
View Journal | View Issue

Cite this: *Chem. Sci.*, 2026, **17**, 1398

All publication charges for this article have been paid for by the Royal Society of Chemistry

Wireless nanopore electrodes (WNEs): from a non-contact conductive tip to applications in electroanalysis and electrocatalysis

Jinjin Li,†[ab] Hengchen Liu,†[a] Ke-Le Chen,[b] Hao-Wei Wang,[b] Juan Tang,*[ab] Yi-Tao Long[b] and Yi-Lun Ying*[b]

Wireless nanopore electrodes (WNEs) exploit bipolar electrochemistry to provide stable and reproducible nanoscale electrochemical interfaces. The conductive material at the nanopore tip serves as a well-defined sensing interface. This feature enables high spatial and temporal resolution while eliminating the need for traditional wire sealing and thereby avoiding noise or instability arising from the contacted electrode. Therefore, the WNE has become a powerful tool in nanoelectrochemistry with broad applications across electroanalysis and electrocatalysis. This perspective outlines the fabrication of closed-type and open-type WNEs and discusses their applications in monitoring the growth of catalytic materials, assessing electrocatalytic activity, and performing intracellular measurements. Special emphasis is placed on their integration with mass spectrometry and optical spectroscopy to achieve multidimensional insights. Finally, we highlight future research directions, focusing on enhancing stability, precise surface functionalization, and the development of miniaturized, portable devices for practical use.

Received 18th August 2025
Accepted 5th December 2025

DOI: 10.1039/d5sc06299c

rsc.li/chemical-science

1. Introduction

Nanoelectrochemistry bridges nanoscale science and electrochemistry,[1–9] enabling direct investigation of charge transfer processes at nanointerfaces with high spatial and high temporal resolution.[10–13] Its unique ability to uncover the interfacial dynamics of electron, proton, and ion transport enables fundamental discoveries and technological innovations in energy conversion and storage,[14] chemical synthesis, sensing,[15,16] and diagnostic technologies.[17,18] By utilizing electrodes with critical dimensions below 100 nm, the nanoelectrode provides a confined sensing interface whose dimensions are matched for detecting single molecules, single nanoparticles or single cells. Therefore, the well-defined sensing interface of the nanoelectrode plays a crucial role in achieving reliable and reproducible measurements, as its precise geometry and surface properties directly govern the signal resolution.[19] A significant challenge remains in developing reproducible, scalable nanoelectrode fabrication methods that ensure both excellent signal integrity (low noise/high reproducibility) and versatile functional capabilities.

Bipolar electrochemistry (BPE) is an electrochemical technique in which a conductive object exhibits spatially differentiated electrochemical activity wirelessly.[20–22] It shows great promise in the fields of materials science and bioanalysis. Upon immersion of a conductive object into an electrolyte solution and subjecting it to an external electric field, a potential gradient forms along its axis, enabling simultaneous oxidation and reduction reactions at opposing extremities.[23,24] The required voltage magnitude is strongly influenced by the dimensions of the conductive object. When the dimensions of the conductive object reach the nanoscale, tens of kilovolts or more are typically required to drive the relevant electrochemical reactions with a redox potential difference of a hundred millivolts in the electrolyte solution. If a nanoscale electrochemical interface exhibits high resistivity, the voltage drop can localize on the confined nano-sized conductive object, producing a substantial polarization potential difference.[25] Solid-state nanopores, including SiNx nanopores and nanopipettes, feature a well-defined nanoscale pore structure at their tips, resulting in electrical resistances typically ranging from the megohm to gigohm scale. The high resistance induces a pronounced voltage drop at the nanopore tip, making it an excellent scaffold for constructing nanoelectrodes based on bipolar electrochemistry. However, these solid-state materials are generally insulating. Coating the nanotip with a conductive layer allows it to be polarized under an applied voltage, thereby forming an electrochemical sensing interface. This design, known as a wireless nanopore electrode, enables the stable and

[a]*National Engineering Research Center for Carbohydrate Synthesis, Key Lab of Fluorine and Silicon for Energy Materials and Chemistry of Ministry of Education, College of Chemistry and Materials, Jiangxi Normal University, Nanchang 330022, China. E-mail: juantang@jxnu.edu.cn*

[b]*Molecular Sensing and Imaging Center, School of Chemistry and Chemical Engineering, Nanjing University, Nanjing 210023, China. E-mail: yilunying@nju.edu.cn*

† These authors contributed to this work.

reproducible generation of a nanoscale electrochemical interface through local polarization of the conductive layer.

In the WNE system, the conductive material within the nanopore functions as a bipolar electrode, enabling simultaneous redox reactions at both ends without a direct electrical connection. The tip of WNEs corresponds to the *cis* side, while the opposite end corresponds to the *trans* side. A pair of electrodes is placed into the electrolyte cell on either side.[26] Compared to traditional nanoelectrodes, where electrode wires are directly encapsulated inside insulated pipettes, the WNE overcomes noise and interface instability caused by defects between the wire and pipette. Moreover, eliminating the physical wire connection between the conductive tip and the external circuit facilitates integration with electrospectroscopy techniques and enables its use as an ion source in mass spectrometry. This feature also simplifies the manipulation of nanoelectrode arrays, thus opening new frontiers in nanoscale applications.

Over the past five years, WNE technology has advanced significantly, evolving from a conceptual approach to practical applications in electroanalysis and electrocatalysis, enabled by its non-contact nature. In this perspective, we first give an overview of the design principle of the WNE with its applications in single-molecule, single-nanoparticle or single-cell detection. We then highlight the integration of wireless nanopore electrodes with complementary techniques such as electrochemiluminescence (ECL), surface-enhanced Raman spectroscopy (SERS), and mass spectrometry to provide multidimensional information, concluding with future perspectives and potential directions for further research in developing portable and intelligent detection instruments.

2. Classification and preparation of wireless nanopore electrodes

Generally, WNEs can be classified into two types—open-type WNEs and closed-type WNEs—depending on the metal structure at the tip.[26] The open-type WNE is modified with conductive materials along with the interior of the nanopore to form a nanoscaled hollow conductor (Fig. 1). When an external potential is applied, faradaic reactions are triggered at both ends of the conductive structure inside the nanopore tip. The hollow cavity of the open-type WNE can serve as a syringe to extract intracellular redox species, while its tip is small enough to penetrate the cell. This conical design minimizes cellular damage, making open-type WNEs well suited for biological applications such as single-cell metabolic analysis.[27]

For the closed-type WNE, the solid conductive object is precisely positioned at the tip of the nanopore to function as a bipolar electrode (Fig. 1). This configuration is then applied for the detection of individual nanoparticles. The conductive object polarized at both ends of the closed-type WNE can be equivalently modelled by two parallel resistor–capacitor (RC) pairs: C_{trans} and R_{trans}, and C_{cis} and R_{cis}. When the voltage is insufficient to oxidize nanoparticles (*e.g.* AuNPs) colliding at the WNE interface, their stochastic interaction perturbs the electric

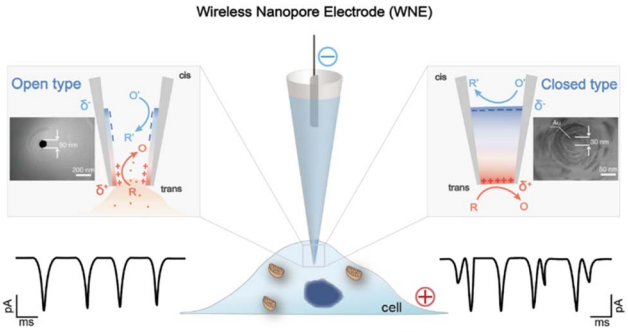

Fig. 1 The design of the WNE for single-entity analysis. The WNE can be classified into two types: open-type (left) and closed-type (right). In the open-type WNE, a conductive layer lines the inner wall of the nanopore, creating a hollow nanoscale conductor where electrochemical reactions occur at both ends under an applied potential. (Inset: SEM image of the open-type WNE). Its hollow cavity can function as a syringe to extract intracellular redox species. In the closed-type WNE, the nanopore tip is filled with a solid conductive material, forming a nanoscale bipolar electrode. (Inset: SEM image of the closed-type WNE). The *trans* side provides a well-defined sensing interface with high temporal and current resolution, enabling sensitive detection of single molecules, nanoparticles, and cells. Reproduced with permission.[28] Copyright 2018, Wiley-VCH. Reproduced with permission.[35] Copyright 2018, American Chemical Society.

double layer ion distribution, causing rapid transient capacitance fluctuations, thereby generating electrical signals.[28] In contrast, collisions with easily oxidized nanoparticles (*e.g.* AgNPs) lead to immediate oxidation, resulting in faradaic currents that dominate the electrochemical response.[29] When a carbon fiber is sealed within a nanopore, with its two ends exposed to different aqueous electrolytes, a bipolar electrochemical circuit forms with a negative Gibbs free energy, generating a measurable potential difference.[30] This principle, known as galvanic redox potentiometry, enables quantitative analysis of redox-active neurochemical targets by recording the potential. We point readers to an excellent review[31–34] for more details on *in vivo* galvanic redox potentiometry.

The WNE is composed of two parts: a solid-state nanopore structure that defines the sensing interface and a nanoscale conductive element that enables electrochemical detection. Various materials are employed for fabricating nanopores, such as a quartz capillary, a two-dimensional membrane (Si_3N_4, SiN_x) and alumina membranes.[36] Strategies have been developed for the preparation of WNEs depending on the material of the nanopore. Typically, the fabrication of a nanopipette-based WNE involves two steps: pulling the quartz capillary and then coating the conductive layer. Multiple methods have been proposed for depositing conductive materials on the nanopipette. We recommend that readers refer to the relevant reviews for more details.[37,38] This perspective provides a summary of the most widely applicable methods.

The laser pulling method is widely used to form nanopipettes due to its ease of preparation and tunable pore size. The process begins with laser-induced melting at the central region of a glass capillary, followed by sequential mechanical pulling to produce two symmetrical nanopipettes. The size of

the nanopipettes can be controlled between 10 and 200 nm by adjusting the pulling parameters.[39] After nanopore formation, the conductive layers such as Au, Ag, or Pt are commonly deposited on the inner walls of the bare nanopipettes using physical vapor deposition techniques like electron-beam evaporation or magnetron sputtering.[40,41] To ensure uniform metal coating, nanopipettes are positioned upright during deposition. In addition, chemical vapor deposition (CVD) is often employed to prepare carbon conductive layers inside nanopipettes.[42] In this approach, a CVD precursor solution is first injected into a glass capillary and dried, followed by carbon deposition on the inner wall *via* CVD using methane as the carbon source and argon as the carrier gas.[43] The thickness and distribution of the carbon layer can be precisely controlled by adjusting the deposition time and gas composition.[44–47] Furthermore, metal salt reduction provides a convenient method to modify solid-state nanopores with metal tips.[48] The nanopipette is initially filled with a metal salt solution, then *in situ* chemical or electrochemical reduction deposits metals such as Ag or Au at the tip, enabling the formation of closed-type WNEs.

WNE arrays can be fabricated by dual-beam focused ion beam (FIB) techniques, lithography and nanoporous alumina templates. Choosing a suitable approach depends on the substrate materials. The dual-beam FIB enables high-precision fabrication of WNE arrays, especially on silicon materials. A 10 × 10 Pt nanopore array was fabricated on a Si_3N_4 film using a dual-beam FIB system.[49] Similar techniques have also been reported on SiN_x membranes to fabricate an Au nanopore array.[50] Although this fabrication method offers appealing precision, it poses a challenge for low-cost and high-throughput fabrication. An alternative strategy is the lithography technique. A Pt nanopore array based on the SU-8 layer was fabricated using this method.[51] In addition, anodized aluminum oxide templates are widely used for fabricating WNE arrays with uniform dimensions.[52]

3. WNEs for single-entity analysis

A WNE incorporating an electrochemically active nanoscale interface within its pore structure enables precise monitoring of the electron/charge transfer process of a single entity. Here, we describe the applications of nanopipette-based WNEs, ranging from single-nanoparticle detection for evaluating catalytic performance to single-cell probing for intracellular measurements, as well as monitoring bioactive species in living organisms.

3.1. Single nanoparticles

By taking advantage of bipolar electrochemistry, a novel silver-coated WNE was developed to serve as a template for electrochemically generating micrometer AuNPs with microcyclic structures.[53] As shown in Fig. 2a, Ag^+ flux, generated from the polarization of the silver nanolayer on the nanopore, can migrate along the inner wall into the solution with a ring-like diffusion profile due to electroosmotic flow. Then, the terminal-alkyne-functionalized gold nanoparticles inside the solution could coordinate with diffused Ag^+, forming the microcyclic structures. The results showed that the size distribution of microcyclic structures is consistent with the Ag^+ electrokinetic diffusion profile. Upon the application of a bias potential, Ag oxidation occurred on the *cis* side, while H^+ reduction generated H_2 bubbles on the *trans* side. H_2 bubbles at the orifice of the nanopore induced a distinct current amplification through nanoconfinement effects of the electric field at the narrowest tip of the nanopore, effectively transforming the faradaic current from the redox process into an easily distinguishable ionic signal (Fig. 2b).[54]

Then, WNEs were applied in single-nanoparticle collision electrochemistry, which holds particular promise for the rapid analysis of single entities in terms of size, aggregation, shape and electrochemical kinetics. A closed-type WNE with a 30 nm gold nanotip was applied to the stochastic collision experiments.[28] Redox-inert nanoparticles (*e.g.* AuNPs) were observed as transient charging-discharging spikes caused by the rapid modulation of the interfacial capacitance as the particle approaches the nanotip. The gold WNE exhibits low noise with a root-mean-square current of 0.6 ± 0.1 pA, and a high temporal resolution of 0.01 ms, thereby achieving a collision frequency over two orders of magnitude higher than that of traditional ultramicroelectrodes. This feature enables *in situ* analysis of mixed nanoparticles with different sizes *via* size-dependent ionic current traces. It provides a new approach to probe ultrafast electrochemical interactions and intrinsic features of nanoparticles (Fig. 2c).

Closed-type WNE platform was also utilized for monitoring the redox-active nanoparticles (*e.g.* AgNPs) with a diameter of 30 nm and 5 nm (Fig. 2d).[29] Compared with classical ultramicroelectrodes, the WNE allows direct detection of both capacitive and electrooxidation signals during nanoparticle collisions. At 0 mV, where the potential is below the oxidation onset, the observed spikes are dominated by capacitive charging. In contrast, at 1 V, the signals become much larger and are mainly governed by the faradaic oxidation of the nanoparticles. Due to the reduced adsorption of the silver nanoparticles on the nanoelectrode surface, the multistep oxidation process of single particles can be recorded. The confinement effect of the WNE tends to repeatedly capture nanoparticles into the tunnelling region until a complete oxidation is achieved. Therefore, this method holds promise in the better understanding of the heterogeneity of single particles.

WNEs have been applied not only for studying electrochemical dissolution but also for exploring the *in situ* electrochemical growth of nanoparticles. Silver salt oxide shows superior oxidation ability for application in superconductivity, sterilization, and catalysis.

However, silver salt oxides are unstable and prone to self-decomposition, which makes characterization difficult. Closed-type WNEs have been used for repeatable growth and dissolution of $Ag_6O_8 \cdot AgHSO_4$.[55] Under a negative potential, silver ions were reduced to form nanoparticles on the cis side, appearing as a bright spot in the dark-field image. Under acidic conditions, applying a positive potential rapidly oxidized the

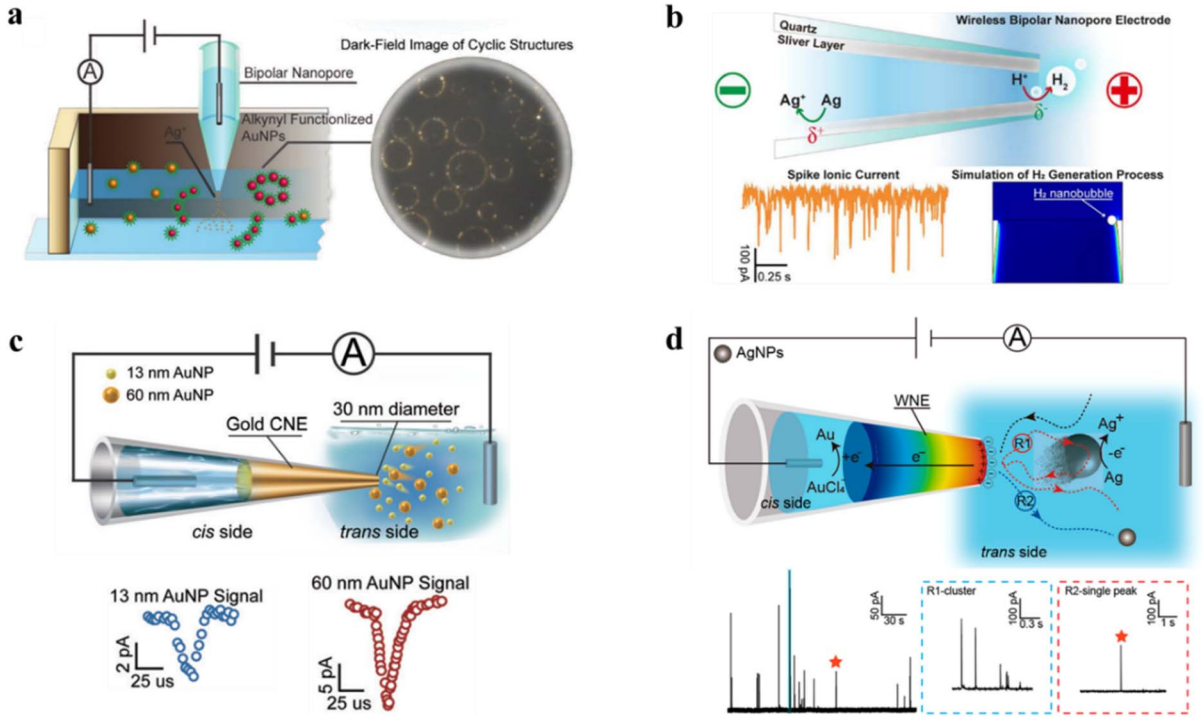

Fig. 2 Applications of WNEs in *in situ* monitoring of nanoparticle growth and dissolution. (a) Schematic illustration of AuNP self-assembly into a microcyclic structure induced by a silver-coated nanopore. By applying a bias voltage, the Ag^+ flux is generated and diffuses from the inner silver-coated nanolayer to the external solution, inducing the self-assembly of alkyne-functionalized AuNPs into microcyclic structures. These homogeneous microcyclic structures were observed under dark-field imaging. (Yellow spheres: 14 nm AuNPs modified with the terminal alkyne compound 5-(1,2-dithiolan-3-yl)-*N*-(prop-2-yn-1-yl) pentanamide, red spheres: terminal alkyne-functionalized AuNPs coordinated with Ag^+). Reproduced with permission.[53] Copyright 2017, Wiley-VCH. (b) Illustration of H_2 and Ag^+ sensing by a silver-coated WNE at the single-particle level. The nanoscale confinement at the WNE tip concentrates the electric field and restricts the diffusion of reaction products, enhancing local ion accumulation. The silver layer is polarized under the applied field, driving H_2 evolution at the cathodic extremity and Ag oxidation at the anodic extremity (top). The orange trace shows the experimental current recorded at −800 mV, while the blue trace represents a simulation of the H_2 generation process. Reproduced with permission.[54] Copyright 2017, American Chemical Society. (c) Revealing the intrinsic and dynamic interactions between single AuNPs and a well-defined 30 nm nanopore electrode. The blue and red spikes are generated from single-nanoparticle collision events of 13 nm and 60 nm AuNPs. In the mixed-system assay, the confined nanopore electrode yields nanoparticle-size-dependent Gaussian current distributions with no overlaps. Reproduced with permission.[28] Copyright 2018, Wiley-VCH. (d) Probing the multistep oxidative process of single AgNP collisions with a WNE (top). The nanoconfinement of the WNE enables the repeated capture of AgNPs from the non-tunneling region into the tunneling region until their complete oxidation. R1 and R2 represent the spike cluster and single-peak signals under 1000 mV, respectively. Spike clusters appear as repetitive peak signals, generated during a multistep oxidation process. They dominate the AgNP collision events on the nanoconfined electrode surface. Only 19% of the oxidation events exhibit single-peak behavior. Reproduced with permission.[29] Copyright 2021, American Chemical Society.

deposited Ag to Ag^+, leading to the formation of $Ag_6O_8 \cdot AgHSO_4$. These particles would catalyze water to produce O_2 as the high valent silver in their structures.

3.2. Single-entity electrocatalysis

Monitoring the catalytic properties of individual electrocatalysts is of importance for rational design. WNEs enable the evaluation of nanocatalyst performance that is otherwise difficult to characterize. For example, the electrocatalytic study of an unstable silver salt oxide (Ag_7NO_{11}) was carried out using closed-type WNEs. The Ag_7NO_{11} catalyst was initially synthesized *in situ* at the nanotip of the closed-type WNE (Fig. 3a).[56] The high-valence silver in Ag_7NO_{11} can oxidize the water to produce O_2, which induced periodic current responses. Real-time current monitoring demonstrated that Ag_7NO_{11}-coated WNE tips exhibited significantly enhanced oxidative activity. The results demonstrate the capability of closed-type WNE for *in situ* assessment of gas–liquid–solid multiphase catalytic reactions, especially for unstable catalysts. The hydrogen evolution reaction is probably the most studied reaction in electrocatalysis. The design and synthesis of highly efficient electrocatalysts is vital for enhancing hydrogen production efficiency. The evolution of H_2 nanobubbles, which is closely related to the catalytic activity of the electrocatalyst, can be detected by the confined space of the nanopore.

A WNE based on C/Pd-Nafion confined in a glass nanopipette was developed to monitor the hydrogen evolution reaction (HER).[57] With a sufficiently negative potential applied to the system, $[Fe(CN)_6]^{4-}$ is oxidized to $[Fe(CN)_6]^{3-}$, while H^+ is reduced to H_2. As shown in Fig. 3b, clear current oscillations were observed from this WNE. Initially, H^+ was reduced to H_2 without bubble formation, leading to a sharp rise in current

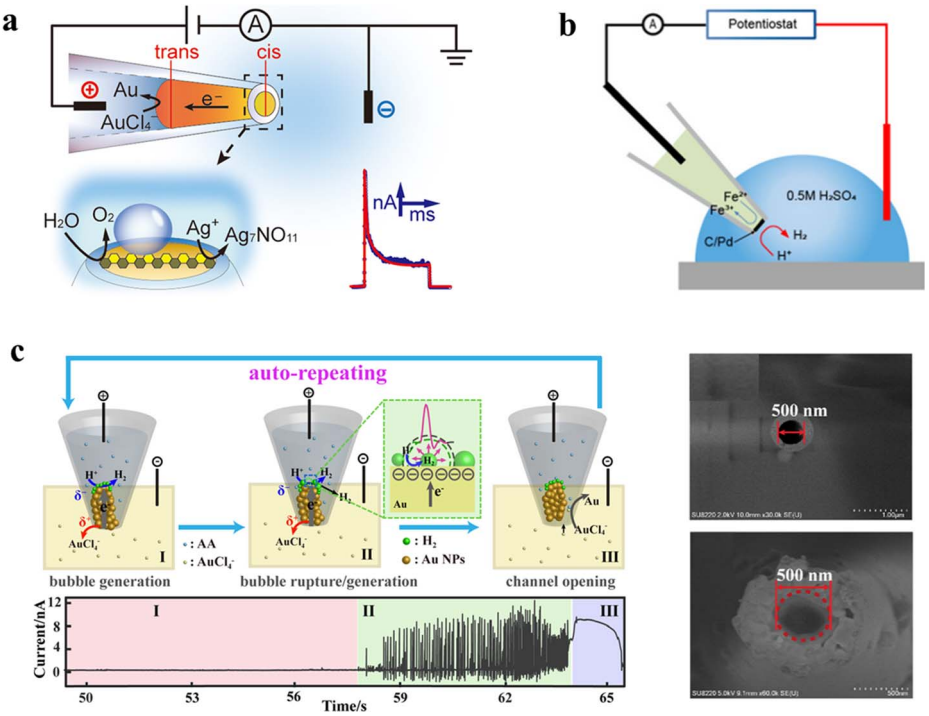

Fig. 3 Single-entity electrocatalytic analysis using WNEs. (a) A closed-type WNE for *in situ* and real-time monitoring of the electrocatalytic performance of Ag_7NO_{11} in the oxygen evolution reaction. Reproduced with permission.[56] Copyright 2022, American Chemical Society. (b) The WNE loaded with a C/Pd catalyst for monitoring the HER. Reproduced with permission.[57] Copyright 2023, Royal Society of Chemistry. (c) Left: monitoring the auto-repeating bipolar reactions and HER on a AuNP-confined WNE: (I) bubble generation, (II) bubble rupture/generation, and (III) channel opening (top). The current–time trace of the first cycle for the AuNP-confined WNE at 1.2 V: (I) the low baseline region, (II) the current pulse region, and (III) the baseline increase region (bottom). Right: SEM image of the orifice with a 500 nm diameter before (top) and after (bottom) blocking the AuNPs. Reproduced with permission.[60] Copyright 2023, American Chemical Society.

that then stabilized. As H_2 became oversaturated in the solution, bubbles began to nucleate on the electrode, causing a sharp current drop due to blockage. Once the bubbles grew large enough to detach from the nanopore, the current increased again. Nanobubbles could continue to grow because the permeability of Nafion ensured a sufficient supply of H^+ to the *cis* side. These current oscillations enable rapid monitoring of bubble generation and release.

Building on this strategy, the catalytic activity of single MoS_2 quantum dots for the HER was investigated by analyzing current blockages from H_2 nanobubbles formed at the WNE tip.[58] MoS_2 QDs and Ag nanoparticles at the nanopipette tip formed a composite bipolar electrode, enabling HER at the MoS_2 sites. The resulting H_2 bubbles produced sharp ionic current blockages on the elevated baseline. Furthermore, the WNE enables electrochemical synthesis of Au nanoparticles confined within a 500 nm tip. As shown in Fig. 3c, the orifice shows a diameter of 500 nm. After the deposition of Au nanoparticles, the orifice was partially blocked. However, this porous structure still allows continuous ionic flow. Under positive potential, the confined AuNPs were electrochemically dissolved on the *trans* side while HER occurs on the *cis* side when the inner solution is acidic, resulting in the periodic current signals. This cyclic process involved: (i) bubble generation. The H_2 bubbles grow and cover the surface of the cathode, hindering the proton transfer, thereby resulting in a low baseline current in Section I. (ii) Bubble rupture and regeneration. Within the confined conical space, bubbles squeeze against one another, leading to their rupture. Once the bubbles rupture, new active electrode surfaces are exposed, enabling protons to rapidly approach the electrode. This triggers an instantaneous increase in the current, forming a positive spike signal. Subsequently, the current drops sharply to the baseline due to the regeneration of new bubbles, which cover the surface of the nanoelectrode. The process is repeated, and many intense current spikes were observed. (iii) Gold nanoparticle dissolution until the channel reopened. AuNPs on the *trans* side continuously undergo oxidation reactions, generating $AuCl_4^-$ and subsequently forming ionic channels. These channels reduce the resistance to ion transport, allowing the current to increase. However, within these channels, $AuCl_4^-$ can regenerate into AuNPs, gradually blocking the channels. This leads to an increase in ion transport resistance, causing the current to correspondingly decay.[60] Therefore, coupled with nanobubble formation and deformation, the WNE can be extended to study the electrocatalytic behavior of various gas-evolving reactions at the single-nanoparticle level.

3.3. *In vivo* single-cell sensing

Real-time monitoring of the dynamics of redox metabolism in living cells is of great importance for understanding cellular communication. To achieve this, a novel asymmetric open-type

WNE with an Au-coated interior was developed.[35] This innovative WNE is capable of real-time detection of redox-active nicotinamide adenine nucleotide (NADH) in a living cell. With the aid of the gold layer, the confined asymmetric geometry can convert the Faraday current response into an easily bubble-induced distinguishable ionic current signal. Specifically, a 90% voltage drop was concentrated at the terminals of the nanopore electrode, attributed to the asymmetric geometry, which converts the Faraday current response into a distinguishable ion current signal. For the detection of NADH, 4-thiol catechol was modified on the gold layer. Its oxidation products can catalyze the oxidation of NADH, promoting nanobubble formation and leading to a pronounced increase in current amplitude. The current resolution of the asymmetric nanopore was greatly enhanced, allowing for the probing of NADH in single living cells with concentrations down to 1 pM (Fig. 4a). Such an asymmetric strategy enables real-time monitoring of the respiratory chain in living cells and assessing the effect of anticancer drugs in single MCF-7 cells.

In addition to the high-sensitivity detection of intracellular analytes, nanopipette-based WNEs can also be used to investigate cellular heterogeneity. For example, an open-type Pt-based WNE was engineered for electro-catalyzing H_2O_2 inside single living cells, generating oxygen with precise control *via* applied voltage (Fig. 4b).[59] Upon insertion into MCF-7 cells, spike-like signals were observed, indicating O_2 nanobubble formation at the nanopipette tip. Furthermore, higher applied voltages resulted in more pronounced quenching of the highly sensitive oxygen probe tris(4,7-diphenyl-1,10-phenanthroline) ruthenium(II) dichloride in MCF-7 cells. These results confirmed the single-cell oxygen manipulation efficacy. Additionally, the hollow structure of the open-type Pt-based WNE enables subcellular-precision drug delivery by combining oxygen generation with direct drug release, thereby alleviating hypoxia-dampened chemotherapy. The electroosmotic force generated by the bias voltage across the nanopipette delivers the drug into the cell. Meanwhile, polarized WNE converts hydrogen peroxide in cancer cells into oxygen. By simultaneously delivering doxorubicin (Dox) and generating oxygen within hypoxic tumor cells, a significant increase in cell-killing efficiency was observed compared to treatment with Dox alone. This platform demonstrated the potential of Pt-based WNE for studying cellular heterogeneity while manipulating the oxygen levels.

The above discussion focused on monitoring current changes under constant applied potential with the WNE. By integrating bipolar electrochemistry, nanopipettes have also been employed for galvanic redox potentiometry (GRP), enabling *in vivo* measurements by recording potential variations at the confined conductive tip.[61–64] This strategy enables sensitive, direct probing of local redox environments. Operating under near-zero-current conditions, GRP minimizes neuronal disturbance and offers a biocompatible approach for *in vivo* neurochemical sensing. As shown in Fig. 5a, a redox-coupled system of $[IrCl_6]^{3-/2-}$ and 5-HT was implemented at the two terminals of a single carbon fiber, achieving real-time monitoring of 5-HT dynamics in the brain.[65] For achieving selective sensing, a carbon fiber electrode was embedded in a glass capillary, with one end modified by phosphorothioate aptamers and the other immersed in a solution of $K_3[Fe(CN)_6]$/$K_4[Fe(CN)_6]$ (Fig. 5b).[66] This aptamer-functionalized GRP (apt-GRP) sensor showed high selectivity for dopamine (DA), even against physiological levels of common interferents. When co-implanting a microelectrode array with an apt-GRP sensor into the striatum of a rat, DA dynamics and electrophysiological signals can be simultaneously monitored in real time in living rat brains. Notably, DA monitoring relies on open-circuit voltage, which allows the system to operate without altering neuronal activity. Therefore, the apt-GR-based WNE platform

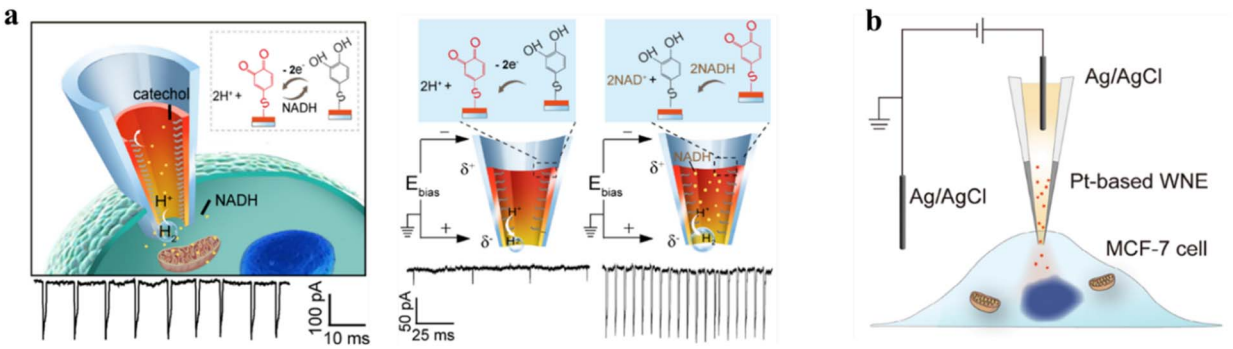

Fig. 4 *In vivo* single-cell sensing with the WNE. (a) Left: schematic of an open-type WNE for monitoring electron transfer processes in a living cell. Right: current responses from a catechol-modified WNE in the absence and presence of NADH. The gold-coated, confined asymmetric geometry of the WNE converts faradaic currents into amplified ionic signals *via* nanobubble generation, enabling distinguishable detection of electron transfer events. In the absence of NADH, the catechol can be electrochemically oxidized to the corresponding *o*-benzoquinone at the anode, whereas H_2 is produced at the cathode. In the presence of NADH, the resulting *o*-benzoquinone is reduced back to catechol, thereby leading to an increased current pulse of high amplitude. All signals were recorded in a 10 mM PBS solution at a bias potential of −0.7 V. Reproduced with permission.[35] Copyright 2018, American Chemical Society. (b) Schematic illustration of the Pt-based WNE with the capabilities of generating oxygen and delivering drugs into single living cells. The Pt layer is polarized under the applied electric field, driving oxygen evolution at the anodic tip. Simultaneously, the electroosmotic flow induced by the bias voltage across the nanopipette transports the drug into the cell through its hollow structure. The resulting oxygen generation alleviates intracellular hypoxia and enhances drug efficacy. Reproduced with permission.[59] Copyright 2024, Wiley-VCH.

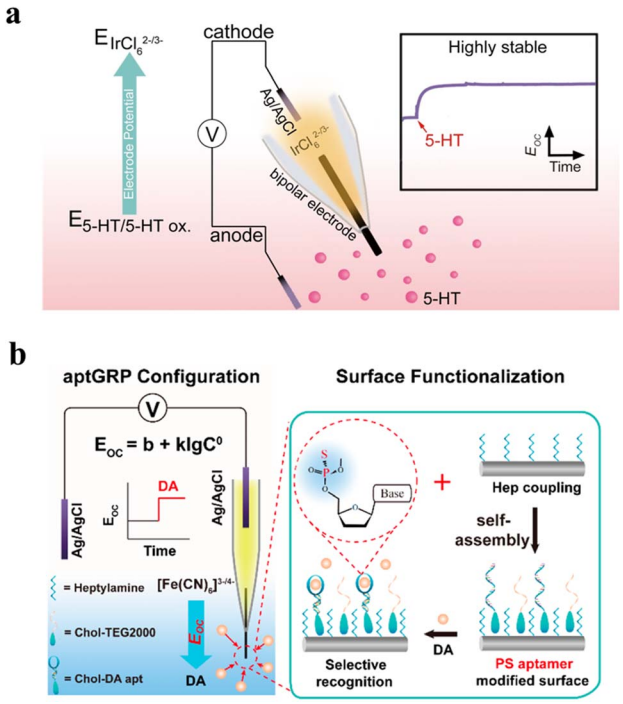

Fig. 5 Galvanic redox potentiometry with the WNE for *in vivo* sensing. (a) Schematic illustration of the $GRP_{5\text{-}HT}$ sensor in the galvanic cell configuration. The redox pair composed of K_2IrCl_6 and 5-HT on the bipolar electrode can spontaneously output steady-state E_{OC}. The anode indicating electrode was placed in the brain containing 5-HT, while the cathode reference electrode was filled with 5 mM K_3IrCl_6/K_2IrCl_6 in the brain. Reproduced with permission.[65] Copyright 2023, Wiley-VCH. (b) Schematic of the GRP sensor for the detection of DA in live rat brains. A carbon fiber was inserted into a glass capillary, with one end immersed in mouse brain regions containing dopamine and the other end placed in a solution of $K_3[Fe(CN)_6]$ and $K_4[Fe(CN)_6]$. In this setup, the aptamer would bring DA near the anode, thereby creating a potential difference between the two sides. The change in open-circuit voltage is related to the concentration of DA. Right: the surface functionalization of the GRP. Heptylamine-modified carbon fiber was obtained from the electrochemical oxidation of heptylamine. Phosphorothioate aptamers were self-assembled onto the heptylamine-functionalized carbon fiber. Reproduced with permission.[66] Copyright 2024, American Chemical Society.

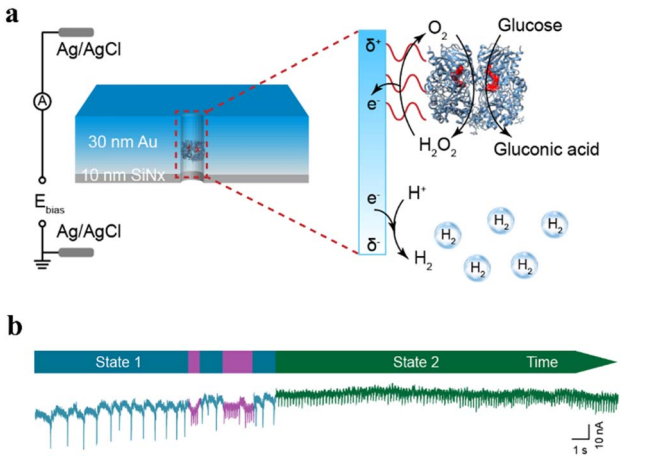

Fig. 6 SiN_x nanopore-based WNE in single-molecule sensing. (a) Schematic illustration of the electrochemical measurement of single enzymes using a SiN_x nanopore, with a cartoon showing a single GO_x showing a "standing" orientation. (b) Raw ionic current traces at −0.8 V in 1 M KNO_3 with 1 mM glucose showing the dynamic catalysis of a single GO_x inside a SiN_x nanopore. The traces show three distinct signal states: state 1 (blue), state 2 (green), and the transient period (purple). Reproduced with permission.[70] Copyright 2023, The Royal Society of Chemistry.

offers a promising strategy for exploring neurotransmission and neural network dynamics *in vivo*. For a comprehensive overview of GRP, please refer to the review articles.[67,68]

3.4. SiN_x nanopore-based WNEs in single-molecule sensing

Generally, the diameter of nanopipette-based WNEs is above 10 nm. For single-molecule sensing, the diameter should match the target molecule. SiN_x nanopores can be fabricated as small as 2 nm,[69] making them suitable for WNEs to probe single enzymatic catalysis dynamics. As shown in Fig. 6a, an open-type gold-coated SiN_x nanopore was prepared by the dielectric breakdown technique.[70] This confined space accommodates a single glucose oxidase (GO_x). Under a highly localized electric field, polarization formed at the pore ends, enabling bipolar electrochemical reactions. At the anode, GO_x oxidizes glucose to gluconic acid, producing H_2O_2. The polarized anode oxidizes H_2O_2 to regenerate O_2, driving the next catalytic cycle. Meanwhile, H^+ reduction at the cathode forms H_2 nanobubbles, causing transient ionic current spikes (Fig. 6b). WNE analysis showed that enzyme orientation inside the nanopore affects the catalysis. A "standing" orientation (state 1) yields higher blockage currents due to greater stability. A "lying" orientation (state 2) improves electron transfer but decreases the catalytic efficiency, resulting in smaller signals. Therefore, this approach opens up possibilities for real-time single-enzyme studies and understanding orientation-dependent activity.

4. WNEs integrated with other techniques

The unique wireless properties and nanoscale spatial confinement of the WNE enable it to work beyond traditional electrochemical detection. Recent advances have demonstrated promising multimodal integrations of WNEs with Raman spectroscopy, mass spectrometry, and various optical techniques, facilitating comprehensive molecular-level information acquisition.

4.1. WNEs with surface-enhanced Raman spectroscopy

By integrating plasmonic metal structures onto the tip of a nanopipette, a plasmonic nanopipette enables SERS-based structural analysis of single molecules. The localized surface plasmon resonance, driven by strong electric field polarization at the plasmonic nanopipette tip, significantly amplifies the electromagnetic field and creates "hot spots".[73] A nanoporous Au sphere was synthesized on the tip of a glass nanopipette to construct a SERS-based sensor for glutathione (GSH)

detection.[71] The nanoporous Au structure exhibited high ionic current rectification and strong SERS activity, attributed to numerous electromagnetic "hot spots". The Au spheres selectively recognized linker molecules, enabling SERS detection of GSH from a single HeLa cell (Fig. 7a). Furthermore, the Au porous sphere linked with i-motif DNA allowed regional pH mapping in single cells. The conformation of the Au porous sphere changed with pH due to folding and unfolding of i-motif DNA. This caused reversible changes in ionic current, potential, and SERS signals, enabling pH probing in different regions of single cells.[74]

Nanopipette-based SERS can also sense protein molecules. For example, an Au plasmonic nanopore monitored the *trans*-location and conformation transition of calmodulin (CaM) by ion current readouts and SERS spectra (Fig. 7b).[72] Two conformers of CaM were distinguished at a single-molecule level. In addition, the SERS results provided structural evidence confirming the interaction between CaM and the plasmonic nanopore. This strategy was further applied to study the unfolding and multistep sequential translocation of the cytochrome c molecule through a SERS-active conical Au nanopore with a sub-10-nm pore size.[75] Therefore, these plasmonic nanopipette sensing platforms based on bipolar electrochemistry achieve dual readouts of electrochemical and SERS signals, enabling multimodal single-entity analysis.

4.2. WNEs as an ion source in mass spectrometry

WNEs have provided sensitive electrochemical signals for single-entity analysis. Recently, their integration with mass spectrometry (MS) has expanded their capabilities by adding a mass-to-charge-based detection mode. MS is a powerful analytical technique characterized by rapid response, high sensitivity, and excellent selectivity, widely used in reaction monitoring and mechanistic studies.[76] However, conventional MS struggles to detect short-lived intermediates *in situ* due to its limited real-time detection under reaction conditions. As an emerging electrochemical-MS hybrid method, WNE can drive faradaic reactions and electrospray ionization wirelessly.[77] This enables the detection of transient intermediates during reactions (Fig. 8a). For example, this approach rapidly transfers electrogenerated species from the electrode–electrolyte interface to the gas phase for MS analysis, capturing microsecond-lived intermediates as $TPrA^{\cdot+}$ (Fig. 8b).

Next, a pair of symmetrically or asymmetrically coated carbon WNEs in parallel was innovatively connected to explore the flash chemistry of electrogenerated reactive intermediates.[78] Several key radical cationic intermediates were identified and confirmed in reactions such as the dehydrogenation dimerization reaction of 8-methyl-1,2,3,4-tetrahydroquinoline (8-methyl-THQ) and the C–H/N–H cross-coupling reaction between DMA and PTA. Furthermore, an alternating current-driven WNE coupled with MS was fabricated to simultaneously detect electrooxidized and electroreduced intermediates. Constantly changing the voltage direction of the alternating current electrolysis enables both electrooxidation and electroreduction intermediates to be detected simultaneously through mass spectrometry. This method captured key intermediates in the C–O/O–H cross-complexation reaction between 4-alkoxyaniline and alcohols.[79]

4.3. Bipolar nanoelectrode array in optical analysis

Bipolar electrochemistry provides a simpler approach to fabricating nanoelectrode arrays because it does not require a direct electrical connection between electrodes and the electroactive interface. Instead, multiple nanoscale metal conductors are driven by an external electric field to enable parallel

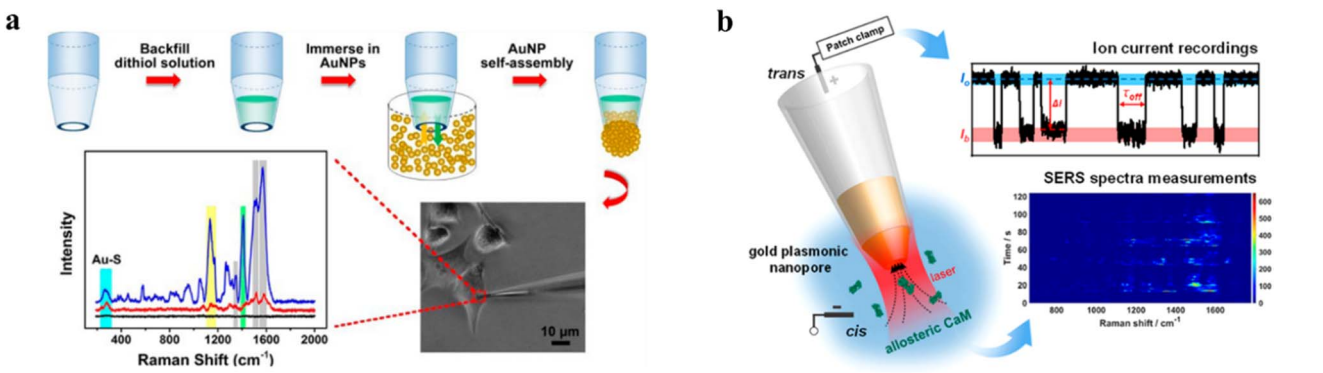

Fig. 7 Surface-enhanced Raman spectroscopy analysis with WNEs. (a) Dual-functional Au nanoporous sphere based nanopore sensing platform with ion current rectification and SERS activity for monitoring glutathione content within single cells. Illustration of the self-assembly of gold nanoporous spheres (GPS) on the tip of a glass nanopipette (top). Micrographs illustrate the insertion of the 1,9-nonanedithiol GPS (C9-GPS) into a living HeLa cell (bottom). The corresponding Raman spectra acquired from the C9-GPS: the black curve corresponds to the sample after plasma treatment, the red curve shows the spectrum recorded following a 10-minute intracellular insertion in a HeLa cell, and the blue curve represents the spectrum after immersion in a 10 mM aqueous GSH solution for 12 hours. Reproduced with permission.[71] Copyright 2017, American Chemical Society. (b) Schematic diagram of the gold plasmonic nanopore for monitoring the allosteric transition of CaM. Two conformers of CaM were clearly resolved at the single-molecule level using both ion current blockade signals and SERS spectra. The current traces (upper right) and a time series SERS spectrum (lower right) of CaM translocation. Reproduced with permission.[72] Copyright 2023, American Chemical Society.

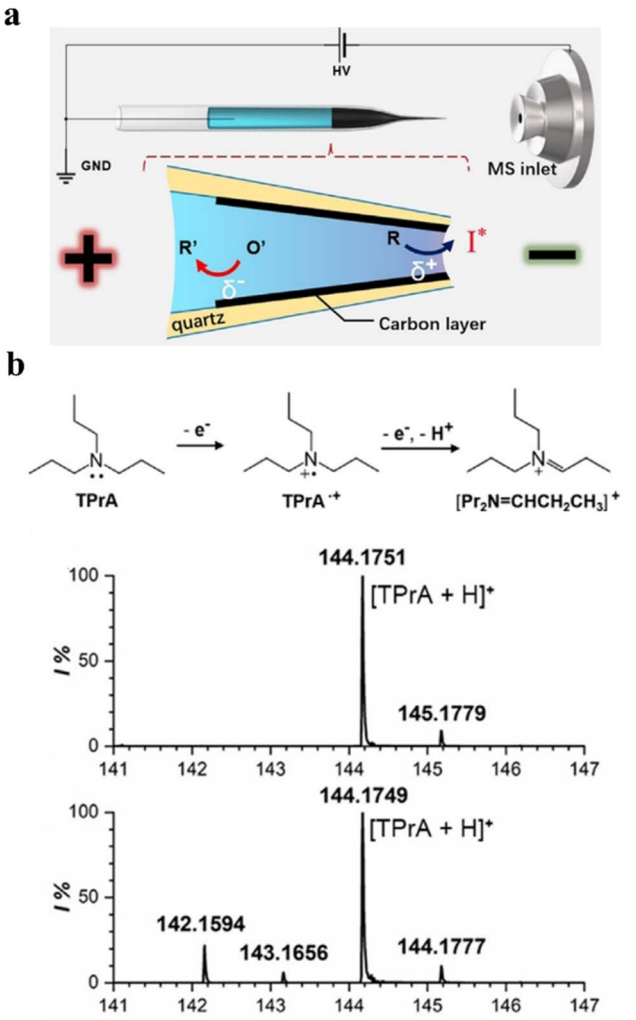

Fig. 8 Mass spectrometry detection using WNEs. (a) Illustration of the combination of the WNE with nano-electrospray ionization mass spectrometry to detect electrogenerated intermediates (bottom). An open WNE is constructed by depositing a thin layer of carbon into the tip of the open-type nanopipette. (b) The mechanism for the electrooxidation of tri-*n*-propylamine (TPrA) (top). Mass spectra of 20 μM TPrA obtained by employing a bare quartz pipette (middle) and the WNE (bottom). Reproduced with permission.[77] Copyright 2020, Wiley-VCH.

measurements. Compared with regular ultramicroelectrodes, WNE arrays avoid the large resistance-capacitance constant and defects caused by wire connection, achieving higher time resolution and lower background noise with obvious advantages. In early studies, Au nanoparticles were selectively deposited on one end of carbon nanotubes in capillaries by bipolar electrochemistry.[80] Later, conductive materials were embedded in pores to create micro-/nano-electrode arrays.[81] At one end, a redox-triggered luminescence reaction converts electrochemical signals into optical readouts. With the anode and cathode in separate chambers, luminescence and sensing occur independently, minimizing background interference. Luminescence is also confined to the nanoelectrode surface, further reducing noise. Wireless bipolar electrode arrays have also been integrated with electrofluorochromism (EFC). Here, a non-fluorescent precursor is converted into a fluorescent product at one terminal, producing an optical signal under laser excitation. Taking advantage of the distinct fluorescence properties of resazurin and Amplex Red before and after the reaction, WNE arrays enable fluorescence imaging of both the anode and cathode.[52] In this example, gold nanoparticles were deposited into porous anodized aluminum oxide to construct EFC sensors, simplifying fabrication and allowing better control of array spacing (Fig. 9a).

In comparison with the EFC method, ECL sensing does not need laser excitation and offers lower background signals. The use of ECL reporting reactions with wireless bipolar nanoelectrode arrays improves sensitivity. Large-scale radiochemical bipolar electrode microarrays were developed early for ECL sensing.[82] Later, a wireless bipolar nanoelectrode array based on a polyethylene terephthalate (PET) membrane was designed to achieve ECL sensing for detecting multiple targets with good performance, such as oxidants, co-reactants, quenchers and biomarkers.[83] Moreover, cellular respiration was also monitored using wireless bipolar nanoelectrode arrays. At the cathode, the local oxygen concentration near the cell aggregates was converted to an ECL signal by $[Ru(bpy)_3]^{2+}$/tripropylamine at the anode (Fig. 9b).[51] Furthermore, the integration of ECL imaging enables visual electrochemical sensing. The array offers high spatial resolution, allowing independent observation of each electrode. For example, they have been used to achieve two-dimensional imaging of epidermal growth factor receptor[84] and to allow sub-micron spatial resolution imaging of the hydrogen evolution reaction of single platinum nanoparticles.[85] Additionally, a FIB method has been proposed to fabricate wireless bipolar nanoelectrode arrays, requiring processing only at one end of a silicon nitride window, thus simplifying manufacturing (Fig. 9c).[49]

5. Perspective

Wireless nanopore electrodes have become a powerful analytical platform distinguished by their wireless operation, enabling facile array fabrication. The high resistance at the nanopore tip concentrates the voltage drop almost entirely across the conductive nanopore material. This ensures that the polarization voltage difference at both ends closely approaches the applied voltage, allowing precise and easy voltage control. The small, tunable nanopore size results in low capacitance and fast current response, offering excellent temporal and current resolution. This size adjustability makes WNEs highly versatile, suitable for detecting single particles, single molecules, and even single cells with nanoscale spatial resolution. Unlike conventional electrodes, WNEs avoid wiring interference and enable simpler instrument design. The relatively straightforward fabrication process also facilitates the preparation of WNE arrays, allowing scalable, multiplexed detection. WNEs can be flexibly integrated with multiple detection modalities, including optical and electrochemical-mass spectrometry methods, further expanding their applicability in analytical and biological studies.

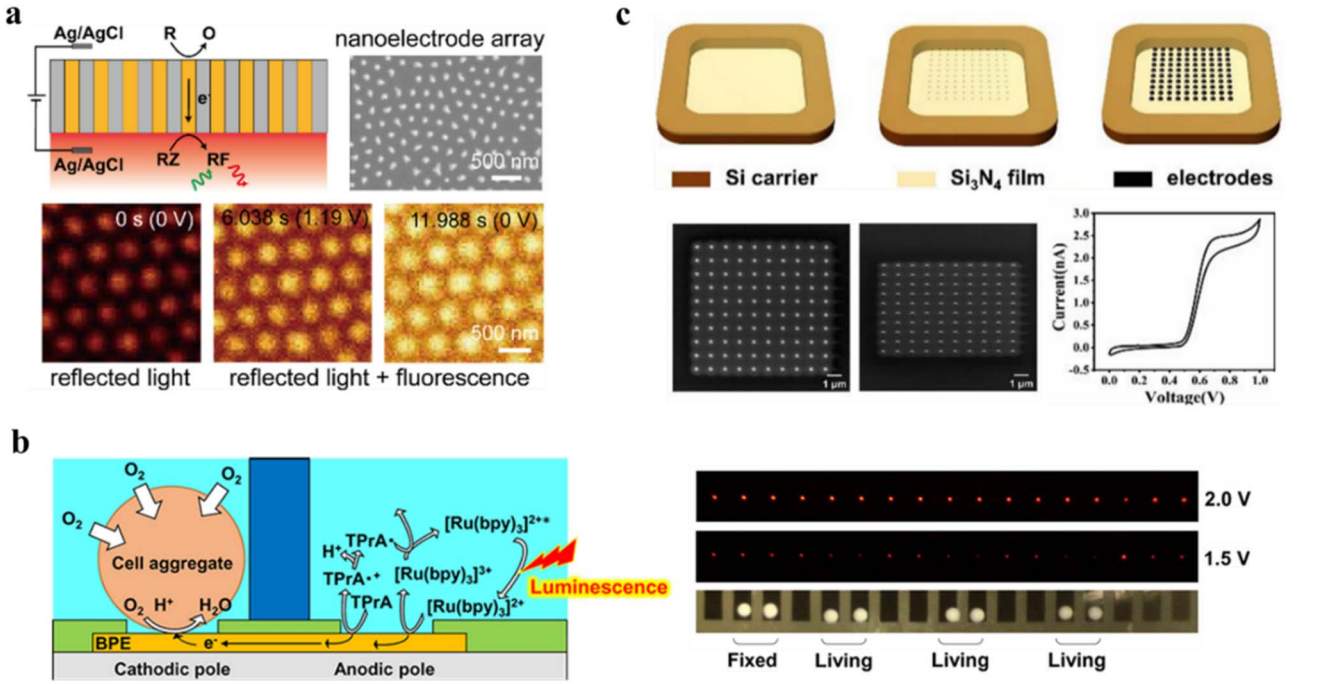

Fig. 9 Bipolar nanoelectrode array in optical analysis. (a) Schematic illustration of an oxidation reaction coupled with an electro-switched fluorescence reaction by the bipolar nanoelectrode array and SEM image of the array (top). Time series of reflectance signals of the electrode array detected by a confocal microscope without a notch filter (bottom). Reproduced with permission.[52] Copyright 2020, American Chemical Society. (b) Schematic illustration and images of ECL-based detection at the BPE for analysis of the respiratory activity of a cell aggregate (left). Optical image of living and fixed cell aggregates at the cathodic poles of the bipolar nanoelectrode array (right). Reproduced with permission.[51] Copyright 2020, American Chemical Society. (c) Schematic of the fabrication of a bipolar nanoelectrode array and helium ion microscopy (HIM) result of a 10 × 10 Pt BPnEA with a spacing of 1 μm (top). Helium ion microscopy image of the above Pt BPnEA array and the corresponding oblique-view HIM image acquired at a 45° tilt angle. Cyclic voltammogram of the BPnEA recorded at a scan rate of 20 mV s^{-1} in an aqueous solution containing 1 M Na_2SO_4 and 1 mM FcMeOH, employing ITO as the working electrode and a homemade Ag/Ag_2O reference electrode (bottom). Reproduced with permission.[49] Copyright 2024, Elsevier.

Despite significant progress, challenges remain, including improving long-term stability and reproducibility, precise control of surface functionalization, and enhancing signal-to-noise ratios in complex biological environments. Parallel to advances in electrode design, efforts toward miniaturized and portable detection instruments continue. For example, arrays of carbon fiber microsensors have been fabricated to achieve high-resolution, simultaneous electrochemical detection of dopamine, ascorbic acid, and ions *in vivo* in rat brains. In parallel, establishing mathematical and physical models that relate the measured current to underlying electrochemical processes is critical for quantitative interpretation and optimization of these sensing platforms.

Building on these advances, the unique structural and wireless features of WNEs present a promising avenue for developing wearable nanopore electrodes. The nanoscale size, inherent wireless operation, and capability for multiplexed array fabrication make WNEs well suited for integration into flexible substrates and portable platforms. Such wearable nanopore electrodes could enable real-time, *in situ* monitoring of biomolecules with high temporal and spatial resolution in complex physiological environments. Key challenges to realize this vision include developing robust materials for long-term skin or tissue contact, ensuring stable and reproducible surface functionalization under dynamic conditions, and optimizing device architectures to maintain high signal-to-noise ratios amidst biological noise. Coupling WNE arrays with miniaturized electronics and wireless data transmission could revolutionize personalized health monitoring and neurochemical sensing. Importantly, WNEs also offer a platform to directly study enzymatic electron/proton transfer mechanisms, opening additional opportunities for enzyme screening, mechanistic investigations, and the design of improved biocatalytic systems.

Looking ahead, the integration of artificial intelligence into WNE systems represents an inevitable trend that will enable smart, autonomous control and multimodal electrochemical sensing with enhanced precision and efficiency.

Author contributions

T. J., Y.-L. Y. and Y.-T. L. conceived the concept of this perspective. J. L., H. L., T. J., Y.-L. Y. and Y.-T. L. wrote the manuscript. J. L., H. L., K. C. and H. W. prepared the figures. All authors contributed to the reviewing and editing of the manuscript.

Conflicts of interest

There are no conflicts to declare.

Data availability

No primary research results, software, or code have been included, and no new data were generated or analysed as part of this perspective.

Acknowledgements

This work was supported by the National Natural Science Foundation of China (22474055, 22366019 and 22334006), the Fundamental Research Funds for the Central Universities (020514380356), and the Natural Science Foundation of Jiangxi Province (20232ACB213011).

References

1 R. M. Penner, M. J. Heben, T. L. Longin and N. S. Lewis, Fabrication and use of nanometer-sized electrodes in electrochemistry, *Science*, 1990, **250**, 1118–1121.
2 V. P. Menon and C. R. Martin, Fabrication and evaluation of nanoelectrode ensembles, *Anal. Chem.*, 1995, **67**, 1920–1928.
3 R. W. Murray, Nanoelectrochemistry: metal nanoparticles, nanoelectrodes, and nanopores, *Chem. Rev.*, 2008, **108**, 2688–2720.
4 Y. Wang, X. Shan and N. Tao, Emerging tools for studying single entity electrochemistry, *Faraday Discuss.*, 2016, **193**, 9–39.
5 J. Clausmeyer and W. Schuhmann, Nanoelectrodes: applications in electrocatalysis, single-cell analysis and high-resolution electrochemical imaging, *Trends Anal. Chem.*, 2016, **79**, 46–59.
6 P. W. Bohn, Science and technology of electrochemistry at nano-interfaces: concluding remarks, *Faraday Discuss.*, 2018, **210**, 481–493.
7 J. Y. Lee, J. h. Park, H. S. Ahn and B. K. Kim, Nanoelectrochemistry for single-droplet analysis and applications, *Curr. Opin. Electrochem.*, 2022, **36**, 101139.
8 Y. Wu, S. Jamali, R. D. Tilley and J. J. Gooding, Spiers memorial lecture. next generation nanoelectrochemistry: the fundamental advances needed for applications, *Faraday Discuss.*, 2022, **233**, 10–32.
9 P. Unwin, Concluding remarks: next generation nanoelectrochemistry-next generation nanoelectrochemists, *Faraday Discuss.*, 2022, **233**, 374–391.
10 O. Wahab and L. A. Baker, Spiers memorial lecture: new horizons in nanoelectrochemistry, *Faraday Discuss.*, 2025, **257**, 9–28.
11 S. H. Huang, M. Parandhaman, S. Farnia, J. Kim and S. Amemiya, Nanoelectrochemistry at liquid/liquid interfaces for analytical, biological, and material applications, *Chem. Commun.*, 2023, **59**, 9575–9590.
12 X. Xu, D. Valavanis, P. Ciocci, S. Confederat, F. Marcuccio, J. F. Lemineur, P. Actis, F. Kanoufi and P. R. Unwin, The new era of high-throughput nanoelectrochemistry, *Anal. Chem.*, 2023, **95**, 319–356.
13 R. Chen, S. Liu and Y. Zhang, A nanoelectrode-based study of water splitting electrocatalysts, *Mater. Horiz.*, 2023, **10**, 52–64.
14 D. W. M. Arrigan, Nanoelectrodes, nanoelectrode arrays and their applications, *Analyst*, 2004, **129**, 1157–1165.
15 P. Ceroni, Y. Chao, C. Crucho, L. De Cola, A. Fucikova, A. Goyal, J. Joo, A. R. Kamali, L. Osminkina, S. Silvestrini, H. Stephan, W. Sun and M. L. Tang, Silicon nanostructures for sensing and bioimaging: general discussion, *Faraday Discuss.*, 2020, **222**, 384–389.
16 R. Wang, G. Qian, J. Guo, Q. Ai, S. Liu, Y. Liu, F. Liang and S. Chang, Nanocollision mediated electrochemical sensing of host-guest chemistry at a nanoelectrode surface, *Faraday Discuss.*, 2022, **233**, 222–231.
17 L. F. Gaudin and C. L. Bentley, Revealing the diverse electrochemistry of nanoparticles with scanning electrochemical cell microscopy, *Faraday Discuss.*, 2025, **257**, 194–211.
18 P. Pandey, A. Sesena-Rubfiaro, S. Khatri and J. He, Development of multifunctional nanopipettes for controlled intracellular delivery and single-entity detection, *Faraday Discuss.*, 2022, **233**, 315–335.
19 Y. T. Long, *Confining electrochemistry to nanopores*, Royal Society of Chemistry, 2020, ISBN:1788012712.
20 R. M. Crooks, Principles of bipolar electrochemistry, *ChemElectroChem*, 2016, **3**, 357–359.
21 L. Bouffier, N. Sojic and A. Kuhn, Capillary-assisted bipolar electrochemistry: a focused mini review, *Electrophoresis*, 2017, **38**, 2687–2694.
22 L. Bouffier, D. Zigah, N. Sojic and A. Kuhn, Bipolar (Bio) electroanalysis, *Annu. Rev. Anal. Chem.*, 2021, **14**, 65–86.
23 K. L. Rahn and R. K. Anand, Recent advancements in bipolar electrochemical methods of analysis, *Anal. Chem.*, 2021, **93**, 103–123.
24 S. E. Fosdick, K. N. Knust, K. Scida and R. M. Crooks, Bipolar electrochemistry, *Angew. Chem., Int. Ed.*, 2013, **52**, 10438–10456.
25 Y. L. Wang, J. T. Cao and Y. M. Liu, Bipolar electrochemistry-a powerful tool for micro/nano-electrochemistry, *ChemistryOpen*, 2022, **11**, e202200163.
26 R. Gao, Y. Lin, Y. L. Ying, Y. X. Hu, S. W. Xu, L. Q. Ruan, R. J. Yu, Y. J. Li, H. W. Li, L. F. Cui and Y. T. Long, Wireless nanopore electrodes for analysis of single entities, *Nat. Protoc.*, 2019, **14**, 2015–2035.
27 Y. Wang, R. Jin, N. Sojic, D. Jiang and H. Y. Chen, Intracellular wireless analysis of single cells by bipolar electrochemiluminescence confined in a nanopipette, *Angew. Chem., Int. Ed.*, 2020, **59**, 10416–10420.
28 R. Gao, Y. L. Ying, Y. J. Li, Y. X. Hu, R. J. Yu, Y. Lin and Y. T. Long, A 30 nm nanopore electrode: facile fabrication and direct insights into the intrinsic feature of single nanoparticle collisions, *Angew. Chem., Int. Ed.*, 2018, **57**, 1011–1015.
29 R. J. Yu, S. W. Xu, S. Paul, Y. L. Ying, L. F. Cui, H. Daiguji, W. L. Hsu and Y. T. Long, Nanoconfined electrochemical sensing of single silver nanoparticles with a wireless nanopore electrode, *ACS Sens.*, 2021, **6**, 335–339.

30 T. Yang, T. Shen, B. Duan, Z. Liu and C. Wang, *In vivo* electrochemical biosensing technologies for neurochemicals: recent advances in electrochemical sensors and devices, *ACS Sens.*, 2025, **10**, 100–121.
31 C. Pan, H. Wei, Z. Han, F. Wu and L. Mao, Enzymatic electrochemical biosensors for *in situ* neurochemical measurement, *Curr. Opin. Electrochem.*, 2020, **19**, 162–167.
32 F. Wu, C. Xu, P. Yu and L. Mao, Galvanic redox potentiometry for *in vivo* sensing, *Biochem. Sens.*, 2021, 453–481.
33 F. Wu, P. Yu and L. Mao, New opportunities of electrochemistry for monitoring, modulating, and mimicking the brain signals, *JACS Au*, 2023, **3**, 2062–2072.
34 J. Lu, X. Zhuang, H. Wei, R. Liu, W. Ji, P. Yu, W. Ma and L. Mao, Enzymatic galvanic redox potentiometry for *in vivo* biosensing, *Anal. Chem.*, 2024, **96**, 3672–3678.
35 Y. L. Ying, Y. X. Hu, R. Gao, R. J. Yu, Z. Gu, L. P. Lee and Y. T. Long, Asymmetric nanopore electrode-based amplification for electron transfer imaging in live cells, *J. Am. Chem. Soc.*, 2018, **140**, 5385–5392.
36 H. Liu, Q. Zhou, W. Wang, J. Zhang and F. Fang, Solid-state nanopore array: manufacturing and applications, *Small*, 2023, **19**, 2205680.
37 R. J. Yu, Y. L. Ying, R. Gao and Y. T. Long, Confined nanopipette sensing: from single molecules, single nanoparticles, to single cells, *Angew. Chem., Int. Ed.*, 2019, **58**, 3706–3714.
38 H. Ma and Y. L. Ying, Recent progress on nanopore electrochemistry and advanced data processing, *Curr. Opin. Electrochem.*, 2021, **26**, 100675.
39 Y. Zhou, L. Sun, S. Watanabe and T. Ando, Recent advances in the glass pipet: from fundament to applications, *Anal. Chem.*, 2022, **94**, 324–335.
40 M. Chang, G. Morgan, F. Bedier, A. Chieng, P. Gomez, S. Raminani and Y. Wang, Review-recent advances in nanosensors built with pre-pulled glass nanopipettes and their applications in chemical and biological sensing, *J. Electrochem. Soc.*, 2020, **167**, 037533.
41 S. Zheng, M. Wu, X. Wang, S. Xu and R. Qian, Nanopipettes for chemical analysis in life sciences, *Chembiochem*, 2025, **26**, e202400879.
42 K. Hu, K. L. Le Vo, A. Hatamie and A. G. Ewing, Quantifying intracellular single vesicular catecholamine concentration with open carbon nanopipettes to unveil the effect of L-DOPA on vesicular structure, *Angew. Chem., Int. Ed.*, 2022, **61**, e202113406.
43 Y. Yu, J. M. Noel, M. V. Mirkin, Y. Gao, O. Mashtalir, G. Friedman and Y. Gogotsi, Carbon pipette-based electrochemical nanosampler, *Anal. Chem.*, 2014, **86**, 3365–3372.
44 M. Wang, J. Liu, X. Liang, R. Gao, Y. Zhou, X. Nie, Y. Shao, Y. Guan, L. Fu, J. Zhang and Y. Shao, Electrochemiluminescence based on a dual carbon ultramicroelectrode with confined steady-state annihilation, *Anal. Chem.*, 2021, **93**, 4528–4535.
45 H. Huang, W. Zhang, M. Li, Y. Gan, J. Chen and Y. Kuang, Carbon nanotubes as a secondary support of a catalyst layer in a gas diffusion electrode for metal air batteries, *J. Colloid Interface Sci.*, 2005, **284**, 593–599.
46 K. Hu, Y. Gao, Y. Wang, Y. Yu, X. Zhao, S. A. Rotenberg, E. Gökmeşe, M. V. Mirkin, G. Friedman and Y. Gogotsi, Platinized carbon nanoelectrodes as potentiometric and amperometric SECM probes, *J. Solid State Electrochem.*, 2013, **17**, 2971–2977.
47 R. Qiu, X. Zhang, H. Luo and Y. Shao, Mass spectrometric snapshots for electrochemical reactions, *Chem. Sci.*, 2016, **7**, 6684–6688.
48 M. Wood and B. Zhang, Bipolar electrochemical method for dynamic *in situ* control of single metal nanowire growth, *ACS Nano*, 2015, **9**, 2454–2464.
49 G. Li and R. Hao, Focused ion beam fabrication of high-resolution electrochemical-electroluminescence coupling bipolar nanoelectrode array sensors, *Sens. Actuators Rep.*, 2024, **8**, 100220.
50 P. Furjes, Controlled focused ion beam milling of composite solid state nanopore arrays for molecule sensing, *Micromachines*, 2019, **10**, 774.
51 K. Ino, R. Yaegaki, K. Hiramoto, Y. Nashimoto and H. Shiku, Closed bipolar electrode array for on-chip analysis of cellular respiration by cell aggregates, *ACS Sens.*, 2020, **5**, 740–745.
52 X. Qin, Z. Q. Li, Y. Zhou, J. B. Pan, J. Li, K. Wang, J. J. Xu and X. H. Xia, Fabrication of high-density and superuniform gold nanoelectrode arrays for electrochemical fluorescence imaging, *Anal. Chem.*, 2020, **92**, 13493–13499.
53 R. Gao, Y. Lin, Y. L. Ying, X. Y. Liu, X. Shi, Y. X. Hu, Y. T. Long and H. Tian, Dynamic self-assembly of homogenous microcyclic structures controlled by a silver-coated nanopore, *Small*, 2017, **13**, 1700234.
54 R. Gao, Y. L. Ying, Y. X. Hu, Y. J. Li and Y. T. Long, Wireless bipolar nanopore electrode for single small molecule detection, *Anal. Chem.*, 2017, **89**, 7382–7387.
55 L. F. Cui, R. J. Yu, H. Ma, P. Hu and Y. L. Ying, Electrically controlled silver salt oxide particle synthesis on a closed wireless nanopore electrode, *Electrochim. Acta*, 2023, **454**, 142348.
56 L. F. Cui, Y. L. Ying, R. J. Yu, H. Ma, P. Hu and Y. T. Long, *In situ* characterization of oxygen evolution electrocatalysis of silver salt oxide on a wireless nanopore electrode, *Anal. Chem.*, 2022, **94**, 15033–15039.
57 L. Tian, J. Liang, Y. Gao, X. Gao and X. Kang, Current oscillations from bipolar nanopores for statistical monitoring of hydrogen evolution on a confined electrochemical catalyst, *Phys. Chem. Chem. Phys.*, 2023, **25**, 7629–7633.
58 S. M. Lu, Y. J. Li, J. F. Zhang, Y. Wang, Y. L. Ying and Y. T. Long, Monitoring hydrogen evolution reaction catalyzed by MoS_2 quantum dots on a single nanoparticle electrode, *Anal. Chem.*, 2019, **91**, 10361–10365.
59 K. L. Chen, R. J. Yu, M. K. Li, H. W. Wang, B. K. Xie, S. C. Liu, Y. L. Ying and Y. T. Long, *In situ* oxygen generation *via* a platinum-based wireless nanopore electrode for single-cell manipulation, *Small Methods*, 2024, **9**, 2401448.
60 S. Bai, Y. You, X. Chen, C. Liu and L. Wang, Monitoring bipolar electrochemistry and hydrogen evolution reaction

of a single gold microparticle under sub-micropipette confinement, *Anal. Chem.*, 2023, **95**, 2054–2061.

61 P. Yu, H. Wei, P. Zhong, Y. Xue, F. Wu, Y. Liu, J. Fei and L. Mao, Single-carbon-fiber-powered microsensor for *in vivo* neurochemical sensing with high neuronal compatibility, *Angew. Chem., Int. Ed.*, 2020, **59**, 22652–22658.

62 C. Pan, F. Wu, J. Mao, W. Wu, G. Zhao, W. Ji, W. Ma, P. Yu and L. Mao, Highly stable and selective sensing of hydrogen sulfide in living mouse brain with NiN_4 single-atom catalyst-based galvanic redox potentiometry, *J. Am. Chem. Soc.*, 2022, **144**, 14678–14686.

63 S. Zhang, W. Ma, Y. Zhang, R. He, J. Wang, P. Yu and L. Mao, Metal/insulator/metal sandwich structure improves background potential stability of galvanic redox potentiometry, *Anal. Chem.*, 2025, **97**, 15790–15797.

64 H. Wei, L. Li, Y. Xue, P. Yu and L. Mao, Stability enhancement of galvanic redox potentiometry by optimizing the redox couple in counterpart poles, *Anal. Chem.*, 2023, **95**, 8232–8238.

65 F. Zhu, Y. Xue, W. Ji, X. Li, W. Ma, P. Yu, Y. Jiang and L. Mao, Galvanic redox potentiometry for fouling-free and stable serotonin sensing in a living animal brain, *Angew. Chem., Int. Ed.*, 2023, **62**, e202212458.

66 J. Ni, H. Wei, W. Ji, Y. Xue, F. Zhu, C. Wang, Y. Jiang and L. Mao, Aptamer-based potentiometric sensor enables highly selective and neurocompatible neurochemical sensing in rat brain, *ACS Sens.*, 2024, **9**, 2447–2454.

67 F. Wu, P. Yu and L. Mao, Multi-spatiotemporal probing of neurochemical events by advanced electrochemical sensing methods, *Angew. Chem., Int. Ed.*, 2023, **62**, e202208872.

68 F. Wu, P. Yu and L. Mao, Analytical and quantitative *in vivo* monitoring of brain neurochemistry by electrochemical and imaging approaches, *ACS Omega*, 2018, **3**, 13267–13274.

69 L. Xue, H. Yamazaki, R. Ren, M. Wanunu, A. P. Ivanov and J. B. Edel, Solid-state nanopore sensors, *Nat. Rev. Mater.*, 2020, **5**, 931–951.

70 R. J. Yu, Q. Li, S. C. Liu, H. Ma, Y. L. Ying and Y. T. Long, Simultaneous observation of the spatial and temporal dynamics of single enzymatic catalysis using a solid-state nanopore, *Nanoscale*, 2023, **15**, 7261–7266.

71 H. L. Liu, J. Cao, S. Hanif, C. Yuan, J. Pang, R. Levicky, X. H. Xia and K. Wang, Size-controllable gold nanopores with high SERS activity, *Anal. Chem.*, 2017, **89**, 10407–10413.

72 W. Li, J. Zhou, Q. Lan, X. L. Ding, X. T. Pan, S. A. Ahmed, L. N. Ji, K. Wang and X. H. Xia, Single-molecule electrical and spectroscopic profiling protein allostery using a gold plasmonic nanopore, *Nano Lett.*, 2023, **23**, 2586–2592.

73 W. Li, J. Zhou, N. Maccaferri, R. Krahne, K. Wang and D. Garoli, Enhanced optical spectroscopy for multiplexed DNA and protein-sequencing with plasmonic nanopores: challenges and prospects, *Anal. Chem.*, 2022, **94**, 503–514.

74 H. Liu, Q. Jiang, J. Pang, Z. Jiang, J. Cao, L. Ji, X. Xia and K. Wang, A multiparameter pH-sensitive nanodevice based on plasmonic nanopores, *Adv. Funct. Mater.*, 2017, **28**, 1703847.

75 J. Zhou, Q. Lan, W. Li, L. N. Ji, K. Wang and X. H. Xia, Single molecule protein segments sequencing by a plasmonic nanopore, *Nano Lett.*, 2023, **23**, 2800–2807.

76 X. Zhang, J. Zhan, Z. Yu, J. Deng, M. Li and Y. Shao, Recent advances in real-time analysis of electrochemical reactions by electrochemical mass spectrometry, *Chin. J. Chem.*, 2022, **41**, 214–224.

77 J. Hu, N. Zhang, P. K. Zhang, Y. Chen, X. H. Xia, H. Y. Chen and J. J. Xu, Coupling a wireless bipolar ultramicroelectrode with nano-electrospray ionization mass spectrometry: insights into the ultrafast initial step of electrochemical reactions, *Angew. Chem., Int. Ed.*, 2020, **59**, 18244–18248.

78 J. Hu, T. Wang, W. J. Zhang, H. Hao, Q. Yu, H. Gao, N. Zhang, Y. Chen, X. H. Xia, H. Y. Chen and J. J. Xu, Dissecting the flash chemistry of electrogenerated reactive intermediates by microdroplet fusion mass spectrometry, *Angew. Chem., Int. Ed.*, 2021, **60**, 18494–18498.

79 X. J. Xi, J. Hu, H. Y. Chen and J. J. Xu, Rapid identification of the short-lived intermediates in alternating-current electrolysis by mass spectrometry, *Chem. Commun.*, 2022, **58**, 10233–10236.

80 C. Warakulwit, T. Nguyen, J. Majimel, M. H. Delville, V. Lapeyre, P. Garrigue, V. Ravaine, J. Limtrakul and A. Kuhn, Dissymmetric carbon nanotubes by bipolar electrochemistry, *Nano Lett.*, 2008, **8**, 500–504.

81 L. P. Zaino, C. Ma and P. W. Bohn, Nanopore-enabled electrode arrays and ensembles, *Microchim. Acta*, 2015, **183**, 1019–1032.

82 K. F. Chow, F. Mavré, J. A. Crooks, B. Y. Chang, R. M. Crooks and A. Large-Scale, Wireless electrochemical bipolar electrode microarray, *J. Am. Chem. Soc.*, 2009, **131**, 8364–8365.

83 Q. Zhai, X. Zhang, Y. Han, J. Zhai, J. Li and E. Wang, A nanoscale multichannel closed bipolar electrode array for electrochemiluminescence sensing platform, *Anal. Chem.*, 2016, **88**, 945–951.

84 J. Gao, H. J. Jin, X. Wei, X. L. Ding, Z. Q. Li, K. Wang and X. H. Xia, Closed bipolar nanoelectrode array for ultra-sensitive detection of alkaline phosphatase and two-dimensional imaging of epidermal growth factor receptors, *ACS Sens.*, 2024, **9**, 3754–3762.

85 X. Qin, Z. Q. Li, J. B. Pan, J. Li, K. Wang and X. H. Xia, Electrochemiluminescence imaging hydrogen evolution reaction on single platinum nanoparticles using a bipolar nanoelectrode array, *J. Electrochem.*, 2021, **27**, 157–167.